Geochimica et Cosmochimica Acta Vol. 54, pp. 1267–1281

0016-7037/90/$3.00 + .00

The formation of leached layers on albite surfaces during dissolution under hydrothermal conditions

ROLAND HELLMANN,[1,*] CARRICK M. EGGLESTON,[2] MICHAEL F. HOCHELLA JR.,[2] and DAVID A. CRERAR[1]

[1]Department of Geological and Geophysical Sciences, Princeton University, Princeton, NJ 08544, USA
[2]Department of Applied Earth Sciences and Department of Geology, Stanford University, Stanford, CA 94305, USA

(*Received April* 6, 1989, *accepted in revised form February* 28, 1990)

Abstract—Hydrothermally altered (225°C) albite was compositionally depth-profiled using X-ray photoelectron spectroscopy (XPS) coupled with calibrated Ar ion sputtering. Solution data were collected during dissolution runs for the same crystals which were spectroscopically analyzed. We found that leached zones depleted in Na, Al, and O develop during the initial, incongruent phase of dissolution. Angle resolved XPS (ARXPS) demonstrated that Na and Al are significantly depleted from the upper few monolayers. Depths of leaching, which range from 10 to 900 Å, decrease with increasing pH in the acid region and increase with pH in the basic region. Based on calculated dissolution rates the depth of leaching can be roughly correlated with the release rate of Si. From the observation that the equivalents of H^+ consumed always exceed the equivalents of Na^+ and Al^{3+} released, hydrolysis cannot be considered to be a simple ion exchange process. The XPS spectra also revealed the presence of Cl^- over the entire leaching depth for samples run at $pH < pH_{zpc}$ (zero point of charge) and Ba^{2+} at $pH > pH_{zpc}$, suggesting electrostatic adsorption of aqueous species at charged sites within the leached layer. The presence of Cl^- and Ba^{2+} also show that preferential leaching creates a porous and open structure which allows for the large-scale influx of solvent molecules. Preliminary evaluations of diffusion transport rates through leached layers suggest that dissolution is not rate limited by diffusion. Instead, the kinetics of dissolution seem to be related to the intrinsic rate of structural hydrolysis. Using the XPS and solution data in conjunction with theoretical and experimental studies in the literature, we propose a dissolution mechanism based on initial ion exchange followed by the hydrolysis of Al and Si, which is modeled as the breakdown of activated complexes formed at bridging oxygen (O_{br}) sites. Elemental mass balances based on comparisons between the XPS and solution data suggest that dissolution occurs non-uniformly and is probably preferentially constrained to dislocations and macroscopic defects within the structure.

INTRODUCTION

HYDROLYSIS REACTIONS OF silicate minerals have been actively studied since the 1930s (TAMM, 1930; CORRENS and VON ENGELHARDT, 1938). The two basic models that have been proposed are well known: one based on diffusion controlled kinetics, and the other based on surface-reaction-controlled kinetics. The diffusion control model stems from silicate dissolution experiments in which the preferential release of alkalis occurred during the initial phase of dissolution, an observation which led to the hypothesis that leached layers form on the surfaces of dissolving minerals and that diffusion of reaction products through leached layers is rate-limiting (e.g., TAMM, 1930; LUCE et al., 1972; CHOU and WOLLAST, 1984, 1985a; and references therein). Mass balance calculations suggested that the thickness of leached layers should be a function of solution pH and temperature, and led to predictions (PAČES, 1973) that leached zones could range in thickness from 370 to 5000 Å at 100–200°C. However, early spectroscopic analyses of silicates reacted at room temperature (both naturally and in the laboratory) did not confirm the presence of leached layers more than a few angstroms thick (PETROVIĆ et al., 1976; HOLDREN and BERNER, 1979; BERNER and HOLDREN, 1979; FUNG et al., 1980; SCHOTT et al., 1981; BERNER and SCHOTT, 1982; SCHOTT and BERNER, 1983). The lack of direct evidence for thick leached layers cast some doubt on the validity of the diffusion model.

The relation between surface area and rate of dissolution (LAGACHE, 1965), as well as the presence of etch pits on reacted surfaces, supports the second model, wherein detachment reactions at the solid/liquid interface control the dissolution rate. Transition state theory has been applied to surface detachment reactions, where the rate-limiting step is the breakdown of activated complexes (RIMSTIDT and BARNES, 1980; LASAGA, 1981a,b; AAGAARD and HELGESON, 1982; HELGESON et al., 1984; MURPHY and HELGESON, 1987). More recently, attention has been focused on modeling interface-controlled reactions as a function of adsorption and formation of surface complexes (SCHINDLER, 1981; SCHINDLER and STUMM, 1987; STUMM and FURRER, 1987; WEHRLI, 1989; and references therein).

Many recent studies, using a variety of spectroscopic techniques, have shown that alteration of surfaces may extend as deep as 1000 Å or more (PETIT et al., 1987a,b, 1990; SCHOTT and PETIT, 1987; NESBITT and MUIR, 1988; MOGK and LOCKE, 1988; CASEY et al., 1988, 1989; ALTHAUS and TIRTADINATA, 1989; GOOSSENS et al., 1989) and that surface compositions may be laterally variable (HOCHELLA et al., 1988a). These observations reopen the question of diffusion versus surface-reaction control and raise new questions con-

* *Present address:* Laboratoire de Géochimie, Université Paul Sabatier-C.N.R.S., 38, rue des Trente-Six Ponts, 31400 Toulouse, France.

cerning repolymerization and other reactions that may occur within leached layers (e.g., BUNKER et al., 1988; CASEY et al., 1988, 1989).

In order to study the formation and properties of leached layers on feldspar, we altered albite crystals at hydrothermal conditions in a flow-through reactor. X-ray photoelectron spectroscopy (XPS), coupled with calibrated Ar ion sputtering, allowed us to obtain compositional depth profiles of altered surfaces as well as limited chemical-state information. We were also able to compare the XPS results directly with solution chemistry results obtained from the same single crystals used in the XPS analyses.

EXPERIMENTAL METHODS AND TECHNIQUES

Amelia albite was chosen for these experiments because it is a compositionally pure endmember albite (e.g., see SMITH and BROWN, 1988). Our electron microprobe analyses of a polished sample verified the stoichiometry ($NaAlSi_3O_8$). The surface areas of representative crystals were measured with a single point BET (Kr−He) method. We used single crystals, rather than powders, to avoid complications from grinding artifacts (e.g., EGGLESTON et al., 1989) as well as to facilitate SEM and spectroscopic examination of the reacted surfaces. The crystals were reacted in a flow-through reactor system constructed almost entirely of high-grade titanium (Fig. 1; details of the apparatus can be found in POSEY-DOWTY et al., 1986). The temperature, pressure, and flow rate were maintained at 225°C, 170 bars, and 2.8 ml/min, respectively; run times ranged from 0.5 to 15 h. These experiments thus cover only the initial stages of incongruent dissolution during which leached layers form. The solution pH's of various runs ranged from 0.57 to 10.1; HCl and $Ba(OH)_2$ solutions were used as the acid and base media, respectively. No attempt was made to exclude atmospheric CO_2. During each run, effluent solution samples were collected and their pH's measured. The concentrations of Na, Al, and Si were measured after acidification using standard ICP and AA techniques. Very low concentration (below 500 ppb) measurements of Si and Al were done colorimetrically (STRICKLAND and PARSONS, 1972; DOUGAN and WILSON, 1974). Based on repeated analyses of samples and standards we determined that at concentrations greater than 500 ppb our estimated analytical accuracy and precision were in the range of 5–10%; at lower concentrations this figure rose to 10–15%.

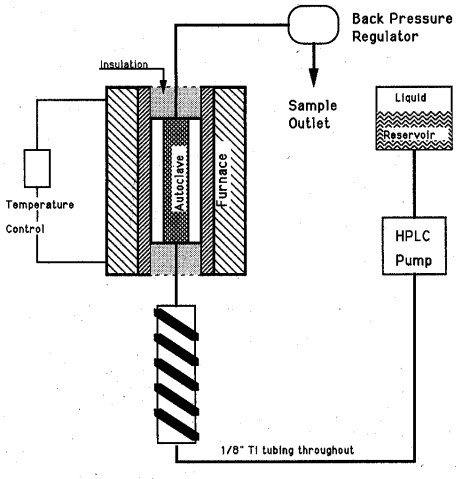

FIG. 1. A schematic diagram of the flow system used, adapted from POSEY-DOWTY et al. (1986). The apparatus was almost exclusively constructed of titanium to limit the effects of corrosion. Inflowing solution was preheated to 180°C (preheater not labeled).

After each run, excess water was blown from the sample with N_2 gas to prevent the precipitation of secondary phases from residual liquid surface films. Because of rapid hydrolysis rates at 225°C, the possibility existed that Al supersaturation was reached with respect to boehmite. Flow rates were maximized (2.8 ml/min) to prevent this. All measured Al concentrations were well below Al saturation limits, based on recent, experimentally-derived, high temperature boehmite solubility curves (BOURCIER et al., 1987). Nevertheless, to check for possible secondary precipitates after dissolution, samples were examined with a Hitachi S-800 field-emission scanning electron microscope operating at 2–3 kV (no coatings were applied).

XPS analyses were conducted on samples both before and after dissolution using a VG ESCALAB Mk II XPS instrument utilizing non-monochromatic Al X-rays (Al Kα = 1486.6 eV). XPS analysis is based on the irradiation of a surface with low energy X-rays and measurement of the kinetic energies of core level electrons ejected from the near surface (see HOCHELLA, 1988, for more information on XPS). Since the mean free paths of photoelectrons ejected by low-energy X-rays are quite short within solids, the detected electrons must therefore originate from the first few atomic layers of the surface. The exact depth of analysis is a function of the attenuation length (λ) of electrons in the solid of interest. We define the analysis depth to be 3λ because 95% of the signal originates from this depth (HOCHELLA, 1988). More specifically, because of the exponential drop-off in signal as a function of depth, 63% of the signal comes from 1λ depth, 86% from 2λ, and 95% from 3λ (see, e.g., HOCHELLA and CARIM, 1988). λ for Si2*p* photoelectrons ejected by Al Kα X-rays traversing amorphous SiO_2 has been accurately measured at 26 Å (HOCHELLA and CARIM, 1988), giving an analysis depth of 78 Å for Si in SiO_2. TANUMA et al. (1988) show that λ is a weak function of composition in oxides, so we estimate that our analysis depth for Si is within 20% of 78 Å. We chose to analyze photopeaks which are near the Si2*p* binding energy so that the λ for all the elements we analyze are within a few Å of each other.

Under the instrument conditions we used, we analyzed a $\approx$10 mm^2 area on each sample, this representing a significant fraction of the total sample surface area. The results thus represent a lateral average of the surface composition. Auger analysis, with micron-scale spatial resolution, of hydrothermally altered feldspars (HOCHELLA et al., 1988a) shows that altered surfaces can be laterally inhomogeneous. This should be kept in mind when interpreting XPS results; we discuss this aspect in more detail later on.

Typical dimensions of the crystal surfaces ranged upwards of 5 × 5 mm, and in each case only the (010) plane was analyzed with XPS in order to assure comparability. CASEY et al. (1988) suggest that the choice of crystallographic plane (for feldspars) is not critical to the determination of leaching depths. Survey scans from 0 to 1000 eV binding energy (BE) at 50 eV pass energy (PE) and 1 eV step size preceeded narrow scans of the Na2*s*, Al2*p*, Si2*p*, and O1*s* peaks at 20 eV PE and 0.1 eV step size. Peak positions were not charge-shift corrected. Peak identities were based on the compilation of WAGNER et al. (1978). Because peak intensities are not directly correlatable to concentrations, due to a photoionization cross-section term, our results are expressed in terms of elemental ratios rather than absolute concentrations. The elemental ratios we present are all normalized to Si because *only* the Si2*p* peak intensity remained relatively constant as a function of depth. Therefore, the ratios show the preferential loss of a given element *with respect* to Si. We have not plotted the ratios as a function of XPS analysis depth; as an example, an XPS analysis of an altered surface *before sputtering* would be plotted at 0 Å, not 80 Å (the analysis depth). Error bars are 95% confidence intervals calculated from replicate XPS analyses of both fresh and altered surfaces.

Angle resolved XPS (ARXPS) was used to gain better depth resolution within the top 80 Å. The analysis depth is a function of the angle between the sample normal and the electron signal collection path, and can be calculated according to the following equation (HOCHELLA, 1988): $d = 3\lambda \cos\theta$, where d is the analysis depth, λ is the attenuation length, and θ is the sample tilt angle. The angles and

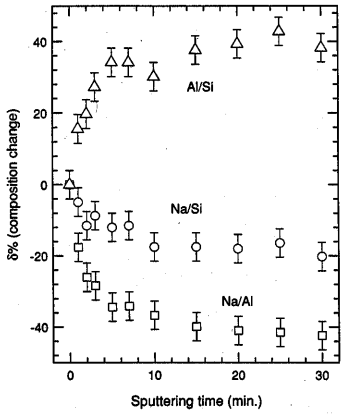

FIG. 2. Variation of the Al/Si, Na/Si, and Na/Al ratios during 30 min of 1 kV Ar^+ sputtering of a homogenous, fresh albite surface. The variations result from Na sputtering at a faster rate than Si, which in turn sputters faster than Al. After several minutes of sputtering, the near-surface composition attains a steady state when the sputtering rate of preferentially removed elements is compensated for by their relative depletion in the near surface. The sputtering profiles for reacted surfaces were compared to these baseline profiles for fresh albite.

the calculated analysis depths were 0° (78 Å), 30° (69 Å), and 65° (34 Å). Thus, by increasing the tilt angle, the sampling depth resolution is increased so that at the largest angle information from only the uppermost 34 Å is obtained.

To obtain compositional depth profiles, the sample surfaces were sputtered with an Ar^+ beam. The sputtering rate (7 Å/min at 1 kV on our gun) was calibrated by sputtering a wafer consisting of a uniform, 64 Å thick thermally grown SiO_2 layer on a Si substrate. XPS analyses were conducted after each sputtering interval. In order to correctly interpret the XPS data, however, differential sputtering must be accounted for. Differential sputtering occurs when certain elements in a multi-component solid sputter faster than others (see HOCHELLA et al., 1988b). We sputtered fresh, homogeneous albite surfaces in order to quantify differential sputtering for albite and to yield calibration curves against which depth profiles of altered samples could be compared. The results are shown in Fig. 2. Real chemical changes in an altered sample are revealed as excursions from these baseline differential sputtering curves.

Our analysis of more than 30 fresh albite cleavage surfaces revealed a range of compositions (especially in Na) which was much greater than the reproducibility of analyses of any one surface. This result is not understood but may be related to the loss of particularly mobile elements like Na from cleavage surfaces which may have experienced incipient leaching. Nonetheless, the magnitude of this fracture effect heterogeneity was insufficient to be mistaken for a leached layer or differential sputtering. To correct for initial differences in composition, the differential sputtering calibration curves were adjusted to match the initial (preleached) Al/Si, Na/Si, and O/Si ratios measured for each surface.

It should also be noted that elemental profiles, obtained by alternating XPS analyses and sputtering, are representative of the true shape of the profile only when the depth of XPS analysis (~80 Å) is very small compared to the depth of compositional change. Otherwise, the profile is a convolution of the depth of XPS analysis with the actual profile. Deconvolution is not possible without making assumptions about the form of the actual profile, which we decided was not defensible. For the purposes of this study, we simply avoid this problem by stating a lower limit on depth resolution at ≈40 Å. Of course, the depth resolution decreases with increases in sputtering depth intervals. However, in some cases (e.g., ARXPS) the depth resolution was higher, on the order of ±10 Å.

Sputtering rates and λs may vary within altered layers. The weak composition dependence of λ in oxides (see above) suggests that the analysis depth in altered layers is similar to that in fresh material. However, the sputtering rate may be somewhat higher than we have measured for amorphous SiO_2. This would cause our leaching depths to be underestimated; i.e., the values we report for leached layer thicknesses may be minima. Sputtering rates are not likely to be more than 20–30% greater than our calibrated rate.

The upper bound on the depth of leaching for any given element is based on the point of intersection of the altered ratio curve with the corresponding calibration curve. The calibration curves do not extend beyond 210 Å depth; we have assumed that steady state for differential sputtering is attained after only 20–50 Å of surface removal, as has been shown by HOCHELLA et al. (1988b). Therefore, the calibration curves have been extended to 1000 Å where necessary in the presentation of the results. In most cases, the data for the depth profiles achieved tangency with the calibration curves. However, when leaching was very pronounced, the curves sometimes never attained tangency with the calibration curves. For example, in Fig. 3 all three ratios plateau at values roughly 15% below the extrapolated calibration curves, which suggests that a common factor is affecting all ratios equally. One explanation is a knock-in effect, in which atoms may be implanted deeper into the solid by Ar^+ impact, and not removed. However, practical experience (e.g., see the sputtering rate calibration above) has shown that the effects of knock-in with sputtering are minimal and at most are capable of causing minor compositional "persistences" over a few tens of angstroms. Other possibilities are

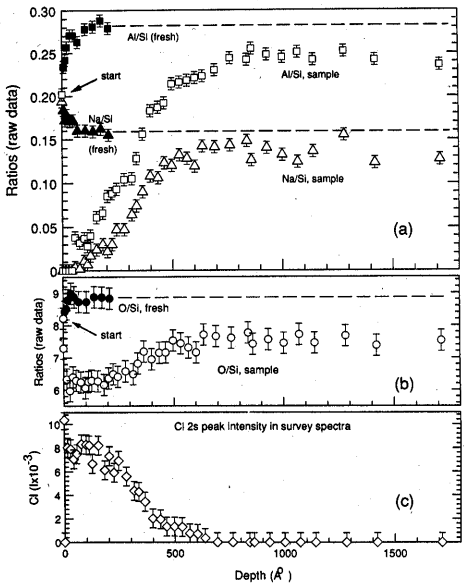

FIG. 3. XPS sputter depth profiling results (open symbols) for a single albite sample reacted at pH 0.57, 225°C for 4 h. The solid symbols represent data from the sputtering of fresh albite (e.g., see Fig. 2) and the dashed lines indicate extensions of these calibration curves. (a) Variations of the Na/Si and Al/Si ratios with depth of sputtering, compared to equivalent curves for fresh albite. (b) Variation of the O/Si ratio with depth. (c) Variation of intensity of the Cl2*s* peak with depth. Error bars are 2σ values calculated from replicate analyses of fresh and altered albite samples.

that the extrapolation of the calibration curves is not valid or that some degree of nonuniform leaching has occurred to depths greater than 2000 Å. A final possibility is that the calibration curves may simply be misplaced by a small amount if the fracture artifacts discussed above gave a slightly anomalous initial surface composition.

RESULTS

Depth profiles

Na/Si, Al/Si, and O/Si ratios are shown in Figs. 3–6 as a function of sputtering depth. Figure 3 shows leaching depths of Na, Al, and O for a sample run at 225°C at pH 0.57 for 4 h. The estimated upper bounds for leaching of Na, Al, and O are 750, 900, and 600 Å, respectively. The uppermost monolayers (~30 Å) are devoid of Na and severely depleted in Al. Over the range from 30 to 1000 Å, the composition of the altered albite gradually approaches that of the unaltered albite. The spectra also revealed the presence of Cl; Fig. 3c shows Cl to a depth of approximately 700 Å. We have no differential sputtering data for Cl, hence the initial drop in Cl intensity after the first sputtering interval may be an artifact of sputtering. However, the gradual decrease in Cl intensity after the initial sputtering period is real. The Cl invasion depth corroborates the leaching depth estimates.

At higher pH's, Na and Al were never completely leached from the near surface, except perhaps in the first monolayer (see ARXPS results below). Fig. 4a,b shows the results for a sample run at pH 2.47 for 7.5 h. The altered surface shows significant depletion in Na to approximately 30 Å depth. The Al/Si ratio at the altered surface is, within uncertainty, the same as for the unaltered, fresh surface. However, depth-profiling revealed that Al depletion occurred to depths of 110–150 Å. The O/Si (Fig. 4b) ratios are slightly lowered with respect to fresh albite in the upper 50–100 Å. Cl did not occur in these spectra. However, another profile for a sample run at pH 2.26 (Fig. 4c) shows Cl gradually decreasing over a range of approximately 200 Å, this equaling approximately

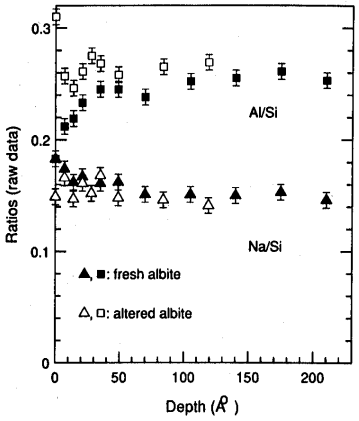

FIG. 5. Variation of the Al/Si and Na/Si ratios (open symbols) compared to fresh albite (filled symbols) with sputtering depth for a sample reacted at pH 5.7, 225°C for 4 h.

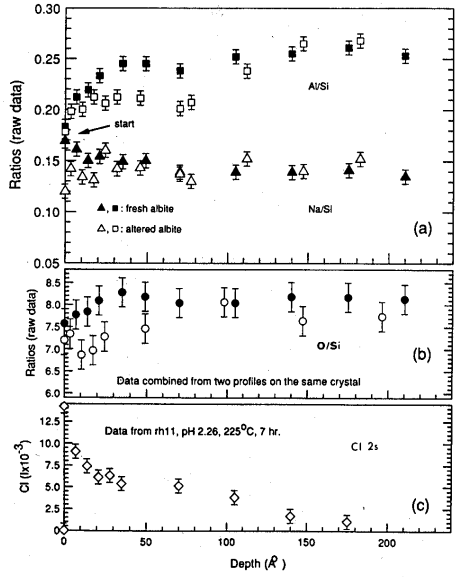

FIG. 4. XPS depth profile results for an albite sample reacted at pH 2.47, 225°C for 7.5 h (open symbols) compared to results for fresh albite (filled symbols). (a) Na/Si and Al/Si depth profiles. (b) O/Si profile. (c) Cl 2s intensity for a separate sample run at pH 2.26, 225°C for 7 h (see text).

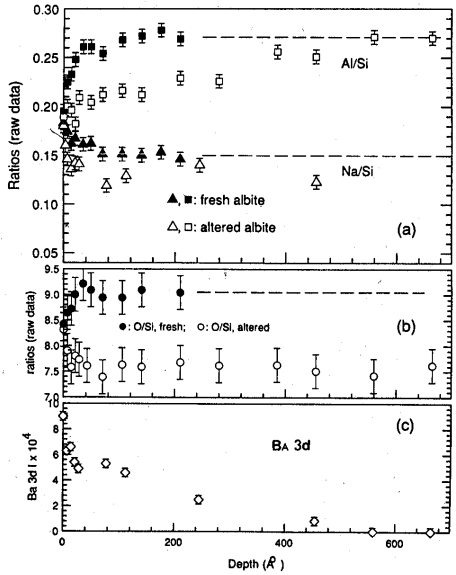

FIG. 6. Depth profiles (open symbols) for a sample reacted at pH 10.1, 225°C for 3.6 h. (a) Al/Si and Na/Si ratios compared to results for fresh albite. (b) O/Si ratio. (c) Intensity of the Ba3*d* peak with depth. Ba infiltration is due to pH adjustment of solution with $Ba(OH)_2$ (see text).

the leaching depth of Al in the sample run at pH 2.47. The significance of the lack of Cl in the spectra for the sample run at pH 2.47 is discussed further on.

Figure 5 shows the results for leaching in a solution of plain water, pH 5.7, at 225°C for 4 h. The surface is depleted in Na to approximately 10–30 Å depth. The Al/Si ratios at the near surface are elevated with respect to fresh albite. The O/Si ratio (not shown) was elevated above that of fresh albite only in the top 10–30 Å.

The sample run at pH 10.1 (Fig. 6) shows Na depletion with respect to Si. The depth of Na leaching is ambiguous, but may be greater than 250 Å. Al/Si ratios show Al depletion roughly to 500–600 Å. O/Si ratios were ambiguous because the ratios never attained tangency with the calibration curve. The solution was pH adjusted with $Ba(OH)_2$, and the XPS results show Ba infiltration to a depth of 500–600 Å, similar to the leaching depth of Al.

The ARXPS analysis of a sample reacted at pH 2.33, 225°C for 14 h is given in Table 1. The Na/Si and Al/Si ratios drop significantly with tilting from 0 to 30°; from 30 to 65°, the change in the ratios is not significant. The full width at half maximum (FWHM) of the O1*s* peaks also drops with increasing tilt angle.

Chemical state trends

Changes in XPS peak shape, binding energy (BE), and full width at half maximum (FWHM) can yield useful chemical state information. Electron BE generally increases with an increase in the formal oxidation state of an element, or with an increase in the electronegativity of attached ligands. The peak shape and FWHM are functions of the number of distinct chemical bonding environments of an atom. Peaks become wider when the number of chemical environments about a certain element increase (e.g., HOCHELLA and BROWN, 1988).

Positions of all elemental peaks scanned in this study were generally shifted by the same amount, indicating that these changes were due to charge shifting. However, changes in peak widths were always observed and are not attributable to charging effects (HOCHELLA, 1988). In most cases the FWHM increased after reaction (measured before sputtering); the observed maximum changes in the FWHM for Na, Al, Si, and O peaks were 1.0, 0.9, 0.4, and 0.7 eV, respectively. This indicates that the atomic structure of altered near-surfaces contain, on average, more unique chemical environments than found within fresh albite. Peak broadening effects induced by sputtering (HOCHELLA et al., 1988b) precluded analysis of the XPS data for chemical state information from the sputtered samples.

Table 1. Angle resolved XPS study of a sample run at pH 2.33, 225°C for 14 hours.

sample description	Na/Si	Al/Si	O1s FWHM
fresh surface	0.173	0.175	2.2
altered, 0° tilt	0.160	0.203	2.3
30° tilt	0.139	0.178	2.2
65° tilt	0.132	0.180	2.0

Solution compositions

The reactor effluent solutions were collected over the course of each experiment. The solution data are presented in terms of effluent concentrations as well as relative release ratios (Figs. 7–9). In order to compare the XPS results with the solution compositions, we have used relative release ratios (RRR) to show the preferential release or retention of Na and Al with respect to Si. A relative release ratio is a measure of the stoichiometric ratio of one element to another in the solution phase, normalized to their ratio in the unaltered solid phase, and are defined in the following manner (HOLDREN and SPEYER, 1985):

$$\log (r.r.r.)_X = \log \frac{\left(\frac{X}{\mathrm{Si}}\right)_{\mathrm{aq}}}{\left(\frac{X}{\mathrm{Si}}\right)_{\mathrm{solid}}} \tag{1}$$

where X = Na or Al. The equations below summarize the three variations that the release ratio can take:

$$\log (r.r.r.)_X = 0: \quad \frac{dX}{dt} = \frac{d\mathrm{Si}}{dt}; \quad \text{congruent} \tag{2}$$

$$\log (r.r.r.)_X > 0: \quad \frac{dX}{dt} > \frac{d\mathrm{Si}}{dt};$$

(+) incongruency, preferential release (3)

$$\log (r.r.r.)_X < 0: \quad \frac{dX}{dt} < \frac{d\mathrm{Si}}{dt};$$

(−) incongruency, preferential retention. (4)

Because all of these experiments were conducted with single crystals in a flow reactor in which there were no appreciable compositional gradients, the effluent concentrations are proportional to the release rates of those elements. The dissolution rate of albite was based on Si, according to the following equation:

$$\frac{CV\,10^{-6}}{M_{\mathrm{Si}}\,\delta_{\mathrm{Si}}\,(SA)} = \text{rate} \quad (\mathrm{mol/cm^2 \cdot s}) \tag{5}$$

where C equals [Si] in mg/L, V is the flow rate in ml/s, M_{Si} is the molecular weight of Si, δ is the stoichiometric normalization factor for Si in albite (=3), and SA is the total surface area (cm^2) (see KNAUSS and WOLERY, 1986, for applicability of this equation).

Figure 7a shows the concentrations of Na, Al, and Si as a function of time for the sample run at pH 0.57 for 4 h at 225°C. Na and Si concentrations do not change significantly after the first 2 h. In contrast, Al concentrations do not show steady state behavior over the course of the experiment. RRR results for Na/Si and Al/Si are shown in Fig. 7b. Here the Al/Si RRR is positive over the entire range of the experiment. This indicates that Al is released preferentially from the albite structure with respect to Si, suggesting that a layer deficient in Al is formed. The XPS results confirm this. The asymptotic approach of the Al/Si release ratio to the congruency line suggests that steady state is approached; we are not certain, however, that overall steady state is achieved.

The Na/Si RRRs (Fig. 7b) are positive during the first hour of the experiment, indicating that Na is also initially preferentially released with respect to Si. At the outset, Na levels

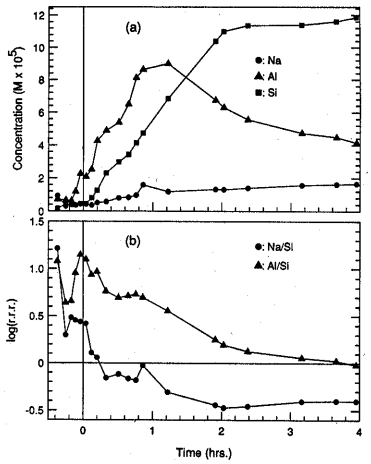

FIG. 7. Solution results. (a) The concentration of Na, Al, and Si in the effluent solutions collected during the reaction of a sample run at pH 0.57, 225°C for 4 h; the corresponding XPS profiles are presented in Fig. 3. (b) Relative release ratios (log *r.r.r.*—see text) calculated from the solution data shown in (a). *Note:* The vertical lines in this and Figs. 8–10 at $t = 0$ represent the time when the reactor reached the desired experimental temperature (225°C). Significant chemical trends take place prior to the attainment of 225°C (to the left of the $t = 0$ line).

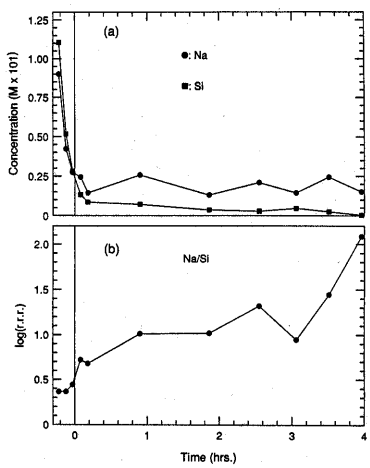

FIG. 8. Effluent Na and Si concentrations and Na/Si release ratios for a sample reacted at pH 5.7, 225°C for 3.6 h. Al concentrations were below the detection limit. Note that the reactor reached 225°C at $t = 0$, shown by the vertical line.

exceed those of Al also. However, during the first hour, the Na release ratio drops below the congruency line, indicating the preferential retention of Na and/or an initially elevated Si release rate. Al release is significantly greater than that of Na during the first hour of dissolution, possibly suggesting that Al is leached to a greater extent.

For the pH 2.47 run (XPS results in Fig. 4), solution data were collected only at the beginning and end of the run. However, the results suggest that the Na/Si RRRs are congruent within the uncertainty of the analyses. The Al/Si RRRs are positive at the end of the experiment, suggesting the preferential leaching of Al. Because many samples were run at acidic pH's (2.1–2.5), we can report the following generalizations. The Al/Si release ratios were mostly positive, whereas the Na/Si ratios were mostly negative. This suggests that either Al is leached to a greater degree or Na is preferentially retained.

The results for the pH 5.7 run (Fig. 8a) show that the initial stages of hydrolysis are marked by elevated Na and Si release rates; these drop to nearly constant values within the first hour of the run. The same results, in terms of RRRs, are shown in Fig. 8b. The Na/Si ratios are positive, indicating the preferential release of Na. The Al concentrations were below the limits of detection; therefore, the Al/Si release ratios are all negative, but indeterminable. Al precipitation as boehmite is unlikely because Al concentrations were well below boehmite saturation (see below). In addition, SEM photomicrographs did not reveal the presence of any precipitates.

At pH 10.1, the solution results (Fig. 9a) show initial high rates of release of Na and Si, with Na showing the most pronounced changes in release rate. However, during the course of the run, all rates were relatively constant, although Al release rates show a broad maximum mid-run. The Na/Si RRRs (Fig. 9b) were consistently positive. The Al/Si RRRs showed similar behavior, with the exception of some irregular initial excursions into the negative field. Taken together, these results indicate that both Na and Al were preferentially leached over the duration of the run.

For all of the samples there was a correlation between initial high positive release ratios and rapid proton consumption,

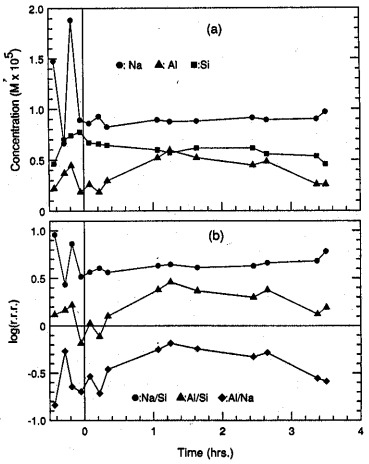

FIG. 9. Effluent Na, Al, and Si concentrations and release ratios for a sample reacted at pH 10.12, 225°C for 3.6 h. Note that the reactor reached 225°C at $t = 0$, represented by the vertical line.

as measured by the difference between the input and output solution pH. A comparison between proton consumption and RRRs can be made by comparing Fig. 10, which shows proton consumption for the sample run at pH 0.57, with Fig. 7a,b. This comparison shows that even though there is a rough similarity between the initially high release rates and release ratios of Na and Al (in particular, Na), there is an observable mismatch between the number of protons consumed and the initial elemental release rates and RRRs; the proton consumption curve remains elevated far beyond the period when Na release rates and RRRs are high. The importance of this is considered below.

DISCUSSION

Our solution and XPS results are generally in accord with the findings of recently published spectroscopic studies of leached layers (see references in Introduction), as well as with the previous feldspar dissolution results of CHOU and WOLLAST (1984, 1985a), WOLLAST and CHOU (1985), and HOLDREN and SPEYER (1985). Below, we discuss some of the differences in our results.

To begin with, the solution data of CHOU and WOLLAST (1984, 1985a) and HOLDREN and SPEYER (1985) indicate the preferential leaching of Na over Al under mildly acidic conditions, whereas we find that Al is leached to greater depths. CHOU and WOLLAST (1984, 1985a) suggest that under basic conditions Si, rather than Al, is preferentially leached. Our experiment at pH 10.1 shows the preferential leaching of Si over Al during the first few minutes of the run; thereafter, Al is leached preferentially. However, our experiment at pH 5.7 showed preferential leaching of Si over Al, this being in general agreement with the SIMS depth profiles of naturally altered plagioclases (under presumably mildly acidic to near neutral conditions) obtained by NESBITT and MUIR (1988). The amount of material leached may not be a simple linear function of the depth of leaching, a possibility which may reconcile some discrepancies. In addition, differences in temperature and/or reaction time may also be a reason for this. Nonetheless, with a few exceptions, our solution and XPS results for hydrothermal conditions agree with those of earlier studies mostly done at room temperature. Given that these leached zones exist, understanding their physical and chemical properties becomes important for the elucidation of the overall hydrolysis reaction.

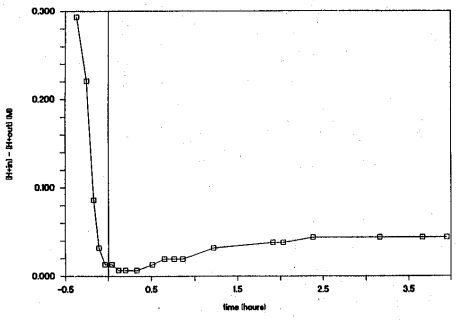

FIG. 10. H^+ (M) consumed during dissolution of an albite sample at pH 0.57, 225°C for 4 h, based on measured input and output pH at 25°C. The approximate correlation between the large H^+ consumption pulse and the high concentrations of Na and Al released at the onset of the experiment suggest rapid surface ion exchange. The region to the left of $t = 0$ represents the initial warm-up period of the reactor, prior to the attainment of 225°C.

Chemical and structural transformations

As mentioned above, the physical and chemical characteristics of the upper-most monolayers of the albite reacted at pH 2.33 were investigated using ARXPS (see Table 1). The Na/Si and Al/Si ratios drop significantly with sample tilting to 30°. The drop in the ratios is consistent with a surface configuration depleted in Na and Al in the uppermost monolayers. The small change in the Na/Si and Al/Si ratios upon tilting from 30 to 65° suggests chemical homogeneity of the depleted near surface to a depth of about 70 Å. The slight broadening of the O1*s* FWHM after leaching is typical of our other samples as well, and is probably the result of adding hydrated O environments to those of albite. These results are also consistent with the measured broadening of O1*s* peaks for altered fayalite by SCHOTT and BERNER (1983). The decline in O1*s* FWHMs with tilting (from 2.3 to 2.0) indicates that the number of chemically distinct O environments decreases towards the surface (HOCHELLA and BROWN, 1988). This simply reflects the loss of Na—O and Al—O environments due to leaching of Na and Al. Further changes in structure deeper than 80 Å undoubtedly occur, but peak broadening effects induced by ion sputtering (HOCHELLA et al., 1988b) obscure hydrolysis effects.

The Si2*p* peaks on the reacted surfaces display a slight asymmetry to the low BE side of the peak and are broadened by 0.4 to 0.5 eV relative to a fresh surface. These effects have been attributed to the presence of SiO_4 tetrahedra not linked at all apices (i.e., the formation of silanol groups), or to changes in electron charge transfer in the Si—O bond due to bond length changes (CARRIÈRE et al., 1977). Analogous arguments apply to Al2*p* broadening. Significant chemical/structural changes are required in order to cause these relatively large changes in FWHMs; however, the application of more specific techniques is needed to aid in the more precise resolution of local atomic environments.

Electron diffraction, TEM, NMR, and Raman studies of laboratory altered glasses and crystalline silicates provide strong evidence that the formation of leached layers is accompanied by amorphization and repolymerization processes (BUNKER et al., 1988; PECK et al., 1988; CASEY et al., 1989; GOOSSENS et al., 1989). Our XPS results are consistent with these studies, and it is thus reasonable to postulate that the loss of Na and Al and the formation of silanol groups leads to a transition from a crystalline to a hydrated, amorphous solid. Our observed changes in the O/Si ratio, from 8:3 (fresh albite) to values approaching 2:1 (silica), strongly support repolymerization processes (BUNKER et al., 1988; CASEY et al., 1988, 1989).

Influx of water

TEM and BET analyses of leached borosilicate glasses by BUNKER et al. (1988) showed evidence for a dramatic increase in surface area and porosity after leaching. H profiles in leached zones of glasses and silicates, obtained using RNR, ERD, and SIMS techniques, show that the total H measured

(H^+, H_2O, OH^-, etc.) is in part due to the migration of molecular water into the structure (PETIT et al., 1987a,b, 1990; SCHOTT and PETIT, 1987; CASEY et al., 1988, 1989; GOOSSENS et al., 1989). Therefore, the disruption and restructuring of the framework suggests the commensurate large scale influx of molecular water.

Our XPS measurements of Cl and Ba peaks show penetration of these solutes to the maximum recorded leaching depths, suggesting the influx not only of water but also of aqueous solutes into the leached structure. Although Cl and Ba may preferentially penetrate to far deeper depths along micro-fractures, dislocation cores, etc., the intensity of the XPS peaks is too great for the Cl and Ba to be restricted to local areas; this means that Cl and Ba must penetrate the leached structure pervasively.

Adsorption and cation balances

In comparing the difference in equivalents of positive charge consumed ($[H^+]_{in} - [H^+]_{out}$) vs. equivalents of positive charge released ($[Na^+] + 3[Al^{3+}]$), it was noted that at low pH more equivalents of positive charge were consumed than released (Table 2). This is an indication that network hydrolysis is not a simple ion exchange process. One explanation for this imbalance in charges is the creation of positive sites within the leached layer. Numerous surface titration studies have shown that positive sites can be created by the addition of H^+ to amphoteric metal—OH groups (see SCHINDLER and STUMM, 1987, and references therein). Hydrolysis of Si—O—Si and Si—O—Al framework bonds results in the formation of Si—OH and Al—OH groups; adsorption of H^+ would create $Al-OH_2^+$ groups at low to intermediate pH and $Si-OH_2^+$ groups at pH < 2. We propose that Cl^- has adsorbed to such positive sites formed during low pH leaching. From our low pH data, we noted that Cl adsorption occurs at pH 2.26, but not at pH 2.47; this suggests that the ZPC can be constrained to a pH ~2.3–2.4, which is within the range of pH_{zpc} values (2.0–2.4) measured for albite (PARKS, 1967). At high pH conditions an analogous argument, invoking negative sites formed during high pH leaching, explains the invasion of the sample run at pH 10.1 by Ba^{2+} (see Fig. 6c).

Adsorption reactions within porous leached zones may thus play a role in the observed aqueous dissolution stoichiometry. For example, Na^+ leached from the albite structure at pH's exceeding the ZPC of the leached zone may not be congruently released to solution due to adsorption at negatively charged sites (e.g., HELLMANN et al., 1989).

Using ERD to measure total H, CASEY et al. (1988) determined that the total H inventory within leached layers in altered labradorite was far less than the equivalents of cations released. This stands in apparent contrast to our proton consumption results. Even though the measurements of H were markedly different, it is difficult to reconcile the differences. In addition, the ERD spectra of Casey and coworkers show

Table 2. Solution data for sample run at pH 0.57, 225°C, 4 hours. Col. 5 gives charge equivalents of Na^+ and Al^{3+} released, and Col. 8 shows equivalents of H^+ consumed. Note that equivalents of H^+ consumed greatly exceeds equivalents of Na^+ and Al^{3+} released. Negative times refer to samples taken during the warm-up period before the experiment reached temperature.

sample	time hours	[Na] Mx10⁵	[Al] Mx10⁵	[Si] Mx10⁵	[Na]+3[Al] Mx10⁵	pHin	pHout	H⁺ cons. Mx10⁵
rh24a	-0.37	0.926	0.704	0.160	3.04	0.57	2.77	29342
b	-0.25	0.291	0.667	0.417	2.29	0.57	1.13	22099
c	-0.17	0.405	0.630	0.377	2.30	0.57	0.68	8619
d	-0.11	0.361	1.186	0.360	3.92	0.57	0.58	3209
e	-0.04	0.426	2.261	0.442	7.21	0.57	0.55	1328
f	0.04	0.418	2.075	0.452	6.65	0.57	0.55	1328
g	0.12	0.361	2.520	0.798	7.92	0.57	0.54	672
h	0.20	0.505	4.262	1.253	13.29	0.57	0.54	672
i	0.33	0.565	4.892	2.307	15.24	0.57	0.54	672
j	0.51	0.796	5.374	2.966	16.92	0.57	0.55	1328
k	0.65	0.826	6.486	3.425	20.29	0.57	0.56	1970
l	0.76	0.957	8.117	4.130	25.31	0.57	0.56	1970
m	0.86	1.579	8.636	4.736	27.48	0.57	0.56	1970
n	1.22	1.183	9.006	6.836	28.20	0.57	0.58	3209
o	1.91	1.318	6.745	10.397	21.55	0.57	0.59	3808
p	2.03	1.305	6.301	11.002	20.21	0.57	0.59	3808
q	2.38	1.396	5.559	11.358	18.08	0.57	0.60	4393
r	3.16	1.57	4.744	11.394	15.80	0.57	0.60	4393
s	3.66	1.622	4.485	11.607	15.08	0.57	0.60	4393
t	3.95	1.653	4.151	11.857	14.10	0.57	0.60	4393

very little penetration of H and virtually no preferential leaching of cations under basic pH conditions. We found that there is a considerable degree of preferential leaching at basic pH conditions. The reason for this discrepancy is not clear; it may, however, be attributable to the lower resolution inherent to the ERD and RBS techniques.

Diffusion control

Given that the formation of leached zones involves the disruption of the structure, rates of ion diffusion should lie intermediate between those in a crystalline solid and an aqueous solution (AAGAARD and HELGESON, 1982). Our XPS data, as well as data from other studies, suggest that a leached zone modeled as a glass is physically not unreasonable. In an attempt to quantify whether diffusional transfer through a leached layer is potentially rate-limiting, we have modeled volume diffusion through a 1000 Å thick slab (corresponding approximately to the thickness of our thickest observed leached layer; see Fig. 3). The model allows us to estimate the fractional losses and concentration profiles of Na and Al in a leached layer.

In the model, the solid is treated both as albite and as two compositionally different glasses (albite and a mixed-Na−Al−Si composition of 14% Na_2O, 14% Al_2O_3, and 72% SiO_2). Diffusion coefficients, based on self-diffusion of Na in these materials, were calculated using the Arrhenius relationship, $D = D_0 \exp(-Q/RT)$. Pre-exponential factors (D_0) and activation energies (Q) for the three phases were obtained from the literature (LIN and YUND, 1972; JAMBON and CARRON, 1976; WILLIAMS and HECKMAN, 1964; respectively). Calculated values for D_{Na} were 10^{-13} for albite and $10^{-9,-10}$ $cm^2\ s^{-1}$ for the albite and mixed glass, respectively. Calculations were made for one dimensional diffusion occuring over 4 h at a temperature of 225°C.

The calculated fractional losses of Na in the slab modeled as albite and the two glasses were 65, 100, and 100%, respectively. The fractional loss calculated from the XPS profile was 35%. Only when time was changed from t = 4 h to t = 15 min did the results based on diffusion through albite match the XPS results. Therefore, the loss of Na by diffusion through 1000 Å of albite (either crystalline or glass) is faster than the experimental rates we observe. The fractional losses of Al, while not calculated, should be approximately of the same order, assuming that $D_{Al} \leq D_{Na}$. Obviously, these calculations should only be viewed as approximate, especially since the variation in leached layer thickness with time is not known. In addition, diffusion coefficients should change continuously through a leached layer, from D_{albite} to D_{glass} (e.g., NESBITT and MUIR, 1988).

Further comparisons were made based on the observed effluent flux of Na at the end of the lowest pH run (see Fig. 7a), and calculated fluxes (based on the XPS profile, Fig. 3a) through a 1000 Å thick leached layer, modeled again as albite and the two types of glass. The fluxes (J) were calculated using Fick's first law, $J = -D(dC_{Na}/dx)$, where a linear $-dC_{Na}/dx$ gradient was derived from the XPS profile. The observed Na flux was on the order of 10^{-11} mol/(cm^2 s); the calculated fluxes through the albite and the two glasses were 10^{-11} and $10^{-6,-7}$ mol/(cm^2 s), respectively. This suggests that only diffusion through unaltered crystalline albite is slow enough to explain our observed fluxes; the leached layers are likely to have much higher diffusion coefficients than crystalline albite. Similar arguments can be made with respect to the flux of hydrogen species *into* the albite structure because the diffusion constants for H_2O in glasses are generally of the same order of magnitude as those for Na (FREER, 1981).

The most important result of these comparisons is that the calculated diffusion transport rates are greater than the measured release rates. The calculated fluxes most probably are conservative estimates because they are based on the thickest leached layer produced in our experiments and are also calculated for a volume diffusion process. Grain boundary, dislocation, and surface assisted diffusion, which may be of considerable importance in dissolution processes, would increase the rates of diffusion by up to several orders of magnitude. In conclusion, our calculations suggest that even though relatively thick leached layers form, diffusion transport through them is not rate-limiting.

Nonuniformity of leaching

The arguments above presuppose that dissolution is uniform over the entire mineral surface. However, sites of high surface strain energy should be preferentially attacked during dissolution, resulting in hydrolysis which is laterally variable (BERNER et al., 1985; CHOU and WOLLAST, 1985b; HOCHELLA et al., 1988a). Evidence for site-specific attack is suggested by the presence of etch pits on reacted surfaces. Figure 11 shows the surface of the sample which was exposed to a pH 0.57 solution for 4 h at 225°C. Trains of deep en-echelon pits have developed over just a small percentage of the overall surface. Because, as we have said, the XPS analyses represent a lateral average surface composition, it is appropriate to assess the magnitude of nonuniform leaching.

From our solution chemistry and XPS results, the contribution of overall leaching vs. localized deep leaching can be roughly estimated. Again using data from Figs. 3 and 7 as a

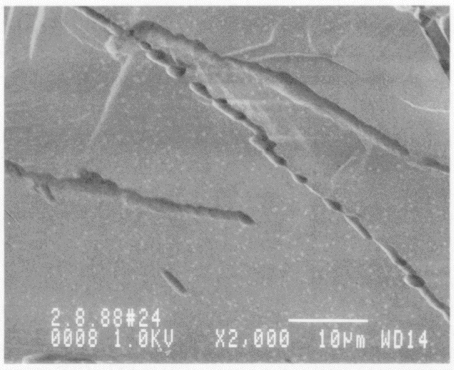

FIG. 11. SEM micrograph at 2000× showing the development of en-echelon etch pits along what appear to be microfractures on the surface of a sample subjected to 4 h of dissolution at 225°C at a pH of 0.57.

basis for calculations, the depth of theoretical Al leaching can be calculated by multiplying the molar volume of albite (100 cm^3/mol) by the total number of moles of Al released and dividing by the surface area. The hypothetical leaching depth of Al, after subtracting the Si leaching depth (the release of Si represents the retreat of the solid/liquid interface), is 4450 Å. The XPS profile for this run (Fig. 3) suggests a depth of only 900 Å for *partial* leaching of Al.

If one simply removed the Na_2O and Al_2O_3 components of albite and collapsed the remaining silica into SiO_2, the volume would decrease to 68% of the original volume. If we now reverse this calculation, assuming 900 Å of residual SiO_2, this should represent 1023 Å of albite. If we further add 30% to this to correct for error in the sputtering rate (see above), this could conceivably represent over 1330 Å of albite. This is still well below the 4450 Å calculated from mass balance. We therefore conclude that the difference must be due to deep leaching along dislocation cores, microcracks, and any other "internal" surfaces not visible to the XPS analyses. Analogous calculations for both Na and Al leaching from all of our samples yielded similar results; that is, 60% to 90% of nonstoichiometric leaching comes from sources which are apparently not XPS visible. In summary, these calculations suggest that leaching at dislocations and microcracks are quantitatively more important than laterally uniform dissolution processes.

PROPOSED MECHANISMS

Ion exchange

Our results show that the first process to occur when albite interacts with water is the rapid exchange of protons (or H_3O^+) for surface-bound Na, as has also been substantiated in numerous studies (e.g., CHOU and WOLLAST, 1984, 1985a). The formation of deep leached layers, however, requires the preferential leaching of Na and Al at considerable depths within the framework. This is dependent on the nature of the solid. PETIT et al. (1989) show that the formation of leached layers is promoted by the presence of mobile network modifiers, such as easily exchangeable alkalis and alkaline-earths. Their study suggests that the formation of leached layers is dependent on ion exchange and water influx being more rapid than the hydrolysis of Si—O groups and their subsequent detachment as silicic acid.

Surface detachment reactions

Following rapid ion exchange of surface bound Na^+, Al—O_{br}, and Si—O_{br} (the br denotes a bridging oxygen), bonds are subject to hydrolysis reactions. To better visualize the initial stages of hydrolysis, we show in Fig. 12a a hypothetical construct of an albite surface, including surface hydroxyls associated with Al and Si atoms (we have omitted exchangeable Na^+ sites). The Si—OH and Al—OH groups are amphoteric and therefore have charges dependent on the solution pH. In Fig. 12 we consider low to intermediate pH conditions ($2 \leq pH \leq 7$), where Si—OH and Al—OH_2^+ groups predominate, based on the zero point of charge (pH_{zpc}), pK_{a1}, and pK_{a2} of Al—OH being 8.5, 7.9, and 9.1, respectively (measured for Al_2O_3; HUANG and STUMM, 1973), and the

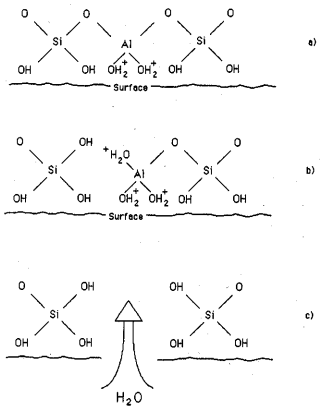

FIG. 12. A hypothetical construct of an albite surface at acid conditions ($pH \geq 2$), showing surface Al—OH_2^+ and Si—OH groups (see text for explanation of charges). One of the Al—O_{br}—Si bonds is preferentially hydrolyzed, resulting in uptake of H^+ and creation of Al—OH_2^+ and Si—OH groups. Further hydrolysis of the Al group breaks the last Al—O_{br} bond, resulting in the detachment of Al from the structure, yielding free $[Al^{3+} \cdot 6H_2O]_{aq}$ and leaving behind another silanol. The overall reaction sequence can be conceived as $2Q^2_{Si} \rightleftharpoons 2Q^1_{Si}$ and $1Q^2_{Al} \rightleftharpoons 1Q^0_{Al}$. Potential further hydrolysis of the Si groups and any possible repolymerization reactions among the silanols are not considered. Note that the detachment of Al leads to restructuring, allowing the influx of water deeper into the structure.

pH_{zpc}, pK_{a1}, and pK_{a2} for Si—OH equaling 2.5, −2.0, and 7.0, respectively (measured for quartz and silica gels; SCHINDLER and GAMSJÄGER, 1972).

The surface charge is important since it has been suggested that the adsorption of H^+ or OH^- to metal—OH groups polarizes and weakens the corresponding metal—O_{br} bonds (FURRER and STUMM, 1986). Therefore, the surface density of weakened metal—O_{br} bonds is a function of solution pH, making the pH dependence of the dissolution rate a function of the number of charged surface sites (e.g., BLUM and LASAGA, 1988). Therefore, we would in general expect the preferential removal of Al, leading to restructuring of the surface and the penetration of water molecules deeper into the structure. This in turn allows access to deeper Na^+ exchange sites and Al sites, where ion exchange and preferential hydrolysis of Al would be repeated; in this way a hydrated silicate layer would result.

The scenario described above is illustrated in Fig. 12a–c. The preferential attack of a partially hydrolyzed Al group results in the uptake of H^+ and the conversion of Al—O_{br} to Al—OH_2^+ and Si—O_{br} to Si—OH groups. The final step is the complete detachment of Al into solution. The detachment of Al allows the influx of water deeper into the structure. For the sake of clarity, we have not considered possible Si—OH condensation reactions. The mechanisms of the Al—O_{br} and Si—O_{br} hydrolysis reactions are discussed below.

The preferential hydrolysis of positively charged groups, such as Al—OH_2^+, has been suggested to occur via a coupled sorption-electrophilic attack mechanism (see LAIDLER, 1965,

p. 594) consisting of rapid nucleophilic adsorption of H^+ (or OH^- at $pH > pH_{zpc}$) at Al—OH sites, followed by the electrophilic adsorption of water dipoles at polarized O_{br} sites, where the subsequent breakage of the Al—O_{br} bond is the rate determining step. Cleavage of the O_{br} bond is speculated to take place by the dissociative chemisorption of the adsorbed water dipole (see BOKSAY et al., 1967, 1968; DE JONG and BROWN, 1980a,b; SMETS and LOMMEN, 1982; MICHALSKE and FREIMAN, 1983). The *pH dependence* of this mechanism is accounted for by the creation of charged metal—OH groups; the subsequent rate determining hydrolysis reactions by water molecules are *pH independent.*

Because the nucleophilic adsorption of H^+ or OH^- involves the creation of 5- or 6-fold coordinated intermediates, the coupled sorption-electrophylic mechanism described above is favored at non-bridging oxygen sites (based on ^{17}O NMR borosilicate glass leaching results from BUNKER et al., 1988). However, the preferential hydrolysis of Al deep within the structure should necessitate the attack of tetrahedrally coordinated Al (Al—O_{br} groups), designated as Q^4_{Al} in Q^n_m notation (where n denotes the number of O_{br} coordinating the central m cation). Based on evidence from glass leaching studies (BUNKER et al., 1988), which suggests that Q^3 and Q^4 species do not readily form intermediates of higher coordination number, a more viable mechanism for breaking highly coordinated Al—O_{br} bonds is based on the direct electrophilic attack of hydrolyzing species at oxygen bridging sites, whereby the *pH dependency* of the process is a function of the *identity of the hydrolyzing species* (e.g., H_3O^+ or H^+, H_2O, OH^-). The direct electrophilic attack of O_{br} sites in Q^4_{Al} and Q^3_{Al} species results in lower-valued Q species, which can then further hydrolyze via the 2-step sorption-electrophilic mechanism, resulting in charged aluminol groups. As noted above, the creation of charged aluminol groups may polarize the remaining Al—O_{br} bonds, making them weaker and more reactive during further hydrolysis reactions. In general, *both mechanisms may be operative* during the preferential leaching and detachment of Al from the structure.

Reactivity of O_{br} sites

The reactivity of O_{br} sites is key to a hydrolysis mechanism based on direct electrophilic attack at O_{br} sites. In an aqueous environment, these O_{br} sites are amphoteric, they can either act as Brönsted acids by accepting electrons, or as p-electron donors (DE JONG and BROWN, 1980a). Molecular orbital (MO) studies of these sites in silicate and aluminate clusters have been carried out and offer not only a reasonably accurate portrayal of the electronic structure and bonding, but also valuable inferences as to their reactivity. The MO studies of DE JONG and BROWN (1980a) are based on calculations involving $H_6T_2O_7^{8-}$ (T = Si, Al) clusters; these clusters are good approximations for the configuration of Si—O—Si and Si—O—Al bonds in solid, 3-dimensional silicate structures (GIBBS, 1982).

According to MO studies, the energetics of reactions vary with the type of molecule (e.g., H_3O^+, H^+, H_2O, or OH^-) approaching the O_{br} site and with the characteristics of the bridging bond associated with the central, coordinating atom. DE JONG and BROWN (1980a) found that the reactivity of O_{br} sites is a function of their non-bonded valence electron density. The charges found on O_{br} in Si—O—Si and Al—O—Al clusters were −4.00 and −4.80, respectively. The greater the density of negative charge, the greater the affinity for hard acceptors (such as H^+) and the more likely that reactive species will chemisorb at O_{br} sites. Therefore, we would expect Al—O_{br} sites to be considerably more reactive than Si—O_{br} sites. In addition, the MO calculations of GEISINGER et al. (1985) show that Al—O_{br} bonds have a smaller Mulliken overlap population than Si—O_{br} bonds and hence are slightly longer than Si—O_{br} bonds (1.695 vs. 1.591 Å), more ionic, and therefore also weaker.

The MO calculations of DE JONG and BROWN (1980b) also consider the energy of interaction between various adion and admolecules (R) and an O_{br} site. They determined that there exists an inverse relationship between the strength of the R—O_{br} bond and the strength of the Si—O_{br} bond. For water and its dissociation products, the energetics of R—O_{br} complex formation were calculated as attachment energies, resulting in the following O_{br} affinity sequence (DE JONG and BROWN, 1980b): H^+ (−317 kcal) > H_3O^+ (−54 kcal) > OH^- (−17 kcal) > H_2O (−9 to −5 kcal). The affinity sequence shows that H^+ has the greatest potential to cleave Si—O_{br} bonds and water molecules the least.

These MO calculations have direct bearing on our experimental results. For example, Fig. 14 shows that the depths of Al leaching are asymmetric in pH; deepest leaching occurs at acid pH, lesser leaching at basic pH, and little leaching at neutral pH. This is consistent with surface-complexation models for the pH dependence of alumina and silica dissolution, and matches qualitatively with MO predictions; i.e., acid species (H^+, H_3O^+) are most reactive, basic species (OH^-) are of intermediate reactivity, and neutral species (H_2O) are least reactive. In addition, the pH dependence of the overall release rate of Si may not only be explainable in terms of a surface complexation/charge density model (e.g., BLUM and LASAGA, 1988) but also may point to an interrelationship between preferential Al leaching, the number of accessible Si—O_{br} sites, and therefore the overall Si release rate (compare Figs. 13–14).

Activated complexes

In discussing the dynamics of bond breakage and reformation during dissolution, we adopt the framework of transition state theory (TST). The overall rate of hydrolysis as well as the preferential leaching of Al is a function of the breakdown of different activated complexes. Considering hydrolysis in an acid medium, a mechanism based on the electrophilic attack of H_3O^+ at an O_{br} site in an Al—O—Si linkage may yield an activated complex $[\ ]^{(*)}$ of the following form:

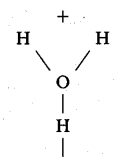

$$\equiv Al-O-Si\equiv + H_3O^+ \rightleftharpoons [\equiv Al-O-Si\equiv]^{(*)} \rightleftharpoons \equiv Al-OH_2^+ + \equiv Si-OH. \quad (6)$$

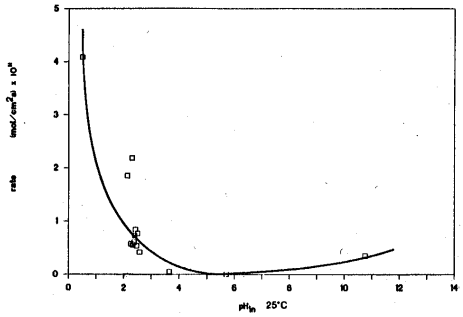

FIG. 13. The dissolution rate of albite, based on Si release, as a function of pH_{in} at 25°C. Similar trends have been observed for many other silicates (BLUM and LASAGA, 1988). We attach no particular mathematical significance to the curve connecting the data points.

It is important to note that TST only describes elementary reactions. In this case, the breaking of the $Al-O_{br}$ bond is the elementary step. The relationship between such elementary steps and the rate of formation of leached layers and the overall rate of hydrolysis is very complex, the explanation of which is beyond the scope of this study. Perhaps the most important point here is that a number of reactions of this type can be written for different possible configurations; they can be written with different species bonded to non-bridging oxygens (O_{nbr}) adjoining O_{br} sites, with Si—O—Si or Al—O—Si linkages, and with different species adsorbing to the O_{br} sites as a precursor to the activated complex. This potential diversity of reaction paths allows for the pH dependence of dissolution.

Even though the exact configurations of the activated complexes are not known, certain configurations are more likely than others. In applying TST to silicate hydrolysis reactions, the activated complex must take into account not only the preferential depletion of alkalis (and other network modifiers) but also the depletion of network forming constituents. TST has been applied to feldspar dissolution by AAGAARD and HELGESON (1982) and HELGESON et al., (1984), who proposed activated complexes of the form $[(H_3O)AlSi_3O_8(H_3O)]^+$ or $[(H_3O)AlSi_3O_7(OH)]^+$ at pH < 2.9 and $(H_3O)AlSi_3O_8(H_2O)_n$ at pH between 2.9–8.0. The breakdown of stoichiometric activated complexes of this type would require not only that many bonds break simultaneously but also the unlikely breakage of $Al-O_{br}$ and $Si-O_{br}$ bonds at the same rate. In addition, the preferential leaching of Al over Si requires different activated complexes for the different Si and Al sites. Thus, it is not clear how the decomposition of these stoichiometric activated complexes could explain the formation of leached zones (i.e., non-stoichiometric residues).

Depolymerization and repolymerization reactions

Activated complexes of the form we propose can be used to describe the depolymerization and repolymerization of the albite aluminosilicate framework during dissolution. We propose that Si and Al must ultimately traverse the depolymerization sequence

$$Q^4_m \Rightarrow Q^3_m \Rightarrow Q^2_m \Rightarrow Q^1_m \Rightarrow Q^0_m \qquad (7)$$

where m may represent either Si or Al. Repolymerization reactions among silanol and aluminol groups, particularly $Q^3_{Si} \Rightarrow Q^4_{Si}$ (i.e., BUNKER et al., 1988), have been omitted. Al species undergo a change from tetrahedral to octahedral coordination in this sequence, but it is reasonable to use this notation to refer to the number of bridging bonds. This sequence is essentially equivalent to the more familiar edge/kink/adatom model commonly invoked for surfaces (e.g., DIBBLE and TILLER, 1981; BLUM and LASAGA, 1987) but with two important differences: first, it makes no assumptions about the structure of the surface (i.e., crystalline, amorphous, reconstructed); second, only detachment of Q^1_m to solution is allowed. That is, $Q^{(n>1)}_m$ species cannot detach directly but are constrained to pass through the Q^1_m state.

If Si—O—Al linkages hydrolyze more quickly than Si—O—Si linkages under all but neutral pH conditions, then Al species must traverse the Eqn. (7) sequence more quickly than Si species, leaving a residual layer of partially depolymerized Q^n_{Si} species which may depolymerize and/or repolymerize according to Eqn. (7). We would expect to observe, within a layer leached of Al, various Q species of Si. Although we have no direct evidence for feldspars, BUNKER et al. (1988) show, using NMR and Raman spectroscopies, that these various Q species, $Q^{4,3,2,1)}_{Si}$, are indeed found in leached silicate structures.

Repolymerization of residual silanol groups via

$$\equiv Si-OH + HO-Si\equiv \Rightarrow \equiv Si-O-Si\equiv + H_2O \qquad (8)$$

and the subsequent removal of water reduces the O/Si ratio within the residual solid; this provides a simple explanation for the reduced O/Si we observe in leached surfaces. Again, although direct evidence for such reactions is lacking for silicate minerals, CASEY et al. (1988, 1989) provide strong indirect evidence and BUNKER et al. (1988) provide convincing

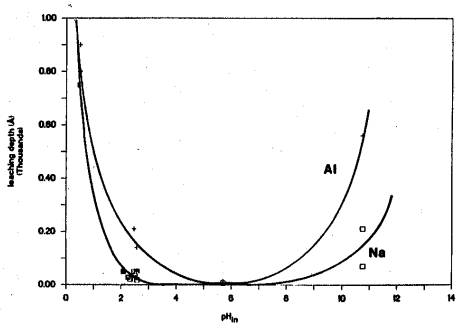

FIG. 14. Depth of Na and Al leaching versus pH_{in} at 25°C. The similarity of this trend with that in Fig. 13 suggests a strong relationship between the depth of leaching and the rate of dissolution, as well as with the identity of the hydrolyzing species at low, intermediate, and high pH (H^+ or H_3O^+, H_2O, OH^-, respectively).

direct evidence for repolymerization in leached silicate glass structures.

Thus, the Eqn. (7) scenario is consistent with spectroscopic studies, with surface complexation models for the pH dependence of reaction rate, and qualitatively with MO predictions. We have not discussed how the sequence of Eqn. (7) could result in our observed rates and stoichiometry, and we have not provided a mechanism by which steady state leached layer thickness could be reached, as is illustrated in Fig. 15. It is clear from Eqn. (7) that, for example, a steady state must be reached between the rate at which Q^1_{Si} are created and the rate at which they are removed by detachment to aqueous solution; this is consistent with our data for Si release in Fig. 7. Similar arguments can be applied to Al release, although the Al release data (Fig. 7) are somewhat more complicated. As mentioned above, the preferential release of Al and the overall rate of Si hydrolysis are probably interdependent. Many different scenarios can be imagined which could account for the observed behavior of dissolution. An assessment of Eqn. (7), for both Q^n_{Al} and Q^n_{Si} species, requires a precise knowledge of the relevant parallel, coupled, and reverse reactions occurring within the leached layer, as well as of the rate-influencing adsorption behavior of aqueous solutes. Such complete information is not yet available.

CONCLUSIONS

This study has resulted in several important observations concerning the formation of leached layers and the mechanisms of dissolution reactions.

1. Leached layers form on albite surfaces during dissolution under hydrothermal conditions. Except at near-neutral pH, both Na and Al are preferentially leached with respect to Si from the albite structure. The thickness of the leached layers is a function of pH.

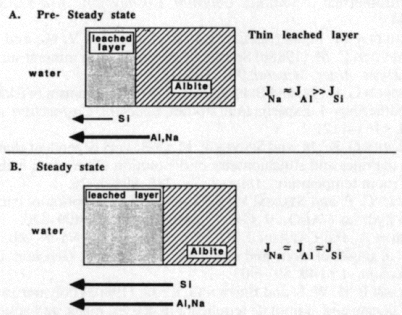

FIG. 15. A simplified representation of leached layer formation. a) Before steady-state is attained, the flux of Na and Al from the surface is greater than the flux of Si because Na—O and Al—O bonds hydrolyze more rapidly than Si—O bonds. The layer thickness increases during this initial period. b) The attainment of a steady state leached layer requires that Na—O, Al—O, and Si—O detachment reactions occur at equal stoichiometric rates. The formulation of an exact mechanism for this is not yet possible due to a lack of knowledge of the relevant parallel, coupled, and reverse reactions occuring within the leached layer.

2. Surprisingly, our XPS data suggest leaching of Al to greater depths than Na, except at neutral pH.
3. During leached layer formation, Cl^- from HCl solutions at pH < pH_{zpc} invades the layer over the entire leaching depth, no Cl^- invades the layer at pH ≥ pH_{zpc}, and Ba^{2+} from $Ba(OH)_2$ solutions invades the layer at pH > pH_{zpc}; this suggests that invasion of leached layers by outside ions is related to adsorption at charged sites within the leached layer. Furthermore, at pH < pH_{zpc} more equivalents of H^+ are consumed than equivalents of Na^+ and Al^{3+} are released, suggesting that $Al{-}OH_2^+$ (and $Si{-}OH_2^+$ at pH < 2) sites form within the leached layer; Cl^- adsorption could occur at these sites.
4. Our calculations suggest that despite the formation of relatively thick leached layers, diffusion of reactants and products through these layers is not rate-controlling.
5. Mass balance calculations show that more Al is released to solution than can be derived from leached layers of the thickness we have observed with XPS; this suggests that the leached layers are non-uniform, and that regions of deep leaching must exist (at dislocations, microcracks, etc.) which have little surface expression.
6. Broadening of XPS peaks for elements in a reacted surface (analyzed before sputtering) indicates an increase in the number of unique chemical environments for these elements over that found in unaltered albite. This probably corresponds to the introduction of hydrogen-containing species within the surface layer.
7. The pH-dependence of release rates and leached layer thicknesses correlate qualitatively with the energetics of interaction of H-containing species ($H^+ > H_3O^+ > OH^- > H_2O$) with bridging oxygen ($O_{br}$) linkages as calculated in MO studies (e.g., DE JONG and BROWN, 1980b).
8. Our observation of reduced O/Si ratios in severely leached layers is consistent with repolymerization reactions in which residual silanol groups (left behind by leaching of Al from the albite structure) within the leached layer react to form siloxane linkages, eliminating oxygen from the structure.
9. Although many variables important to the kinetic description of leached layer formation are unknown, it is possible, using TST and information on the reactivity of O_{br} sites, to qualitatively describe the formation of leached layers without resorting to diffusion rate control.

Acknowledgments—We gratefully acknowledge the use of the SEM facilities at the Center for Integrated Systems and the XPS facility at the Center for Materials Research at Stanford University. We also would like to thank the following Princetonians for assistance with various parts of this study: Maria Borcsik, Ted Forseman, Charles Kulick, Cameron Davidson, and Elaine Lenk. Discussions with Adam Ellison and David Phillips proved very helpful. We also thank David Phillips for use of his diffusion modeling code. Informal comments by A. Navrotsky and W. H. Casey, as well as formal reviews by M. A. Velbel, D. W. Mogk, and an anonymous reviewer considerably aided us in improving the manuscript. Financial support for this project was through Stanford's Center for Materials Research and the Chevron Oil Field Research Company for M.F.H. and NSF grants EAR-8218726 and EAR-8407651 to D.A.C., who also gratefully acknowledges financial support from the Shell Companies Foundation. C.M.E. acknowledges support from an NSF graduate fellowship and from the McGee Fund (Stanford School of Earth Science), and ded-

icates his contribution to the memory of Noye M. Johnson of Dartmouth College. Culinary support from the Prolific Oven.

Editorial handling: G. R. Holdren Jr.

REFERENCES

AAGAARD P. and HELGESON H. C. (1982) Thermodynamic and kinetic constraints on reaction rates among minerals and aqueous solutions. I. Theoretical considerations. *Amer. J. Sci.* **282,** 237–285.

ALTHAUS E. and TIRTADINATA E. (1989) Dissolution of feldspar: The first step. In *Water-Rock Interaction WRI-6* (ed. D. L. MILES), pp. 15–17. A. A. Balkema.

BERNER R. A. and HOLDREN G. R. JR. (1979) Mechanism of feldspar weathering—II. Observations of feldspars from soils. *Geochim. Cosmochim. Acta* **43,** 1173–1186.

BERNER R. A. and SCHOTT J. (1982) Mechanisms of pyroxene and amphibole weathering—II. Observations of soil grains. *Amer. J. Sci.* **282,** 1214–1231.

BERNER R. A., HOLDREN G. R. JR., and SCHOTT J. (1985) Surface layers on dissolving silicates. *Geochim. Cosmochim. Acta* **49,** 1657–1658.

BLUM A. E. and LASAGA A. C. (1987) Monte Carlo simulations of surface reaction rate laws. In *Aquatic Surface Chemistry: Chemical Processes at the Particle-Water Interface* (ed. W. STUMM), pp. 255–292. J. Wiley & Sons.

BLUM A. E. and LASAGA A. C. (1988) Role of surface speciation in the low-temperature dissolution of minerals. *Nature* **331,** 431–433.

BOKSAY Z., BOQUET G., and DOBOS S. (1967) Diffusion processes in the surface layer of glass. *Phys. Chem. Glasses* **8,** 140–144.

BOKSAY Z., BOQUET G., and DOBOS S. (1968) The kinetics of the formation of leached layers on glass surfaces. *Phys. Chem. Glasses* **9,** 69–71.

BOURCIER W. L., KNAUSS K. G., and JACKSON K. J. (1987) Aluminum hydrolysis constants to 250°C determined from boehmite solubility measurements (abstr.). *Geol. Soc. Amer. Abstr. Prog.* **19,** 596.

BUNKER B. C., TALLANT D. R., HEADLEY T. J., TURNER G. L., and KIRKPATRICK R. J. (1988) The structure of leached sodium silicate glass. *Phys. Chem. Glasses* **29,** 106–120.

CARRIÈRE B., DEVILLE J. P., BRION D., and ESCARD J. (1977) X-ray photoelectron study of some silicon-oxygen compounds. *J. Electron Spec. Relat. Phenom.* **10,** 85–91.

CASEY W. H., WESTRICH H. R., and ARNOLD G. W. (1988) Surface chemistry of labradorite feldspar reacted with aqueous solutions at pH = 2, 3, and 12. *Geochim. Cosmochim. Acta* **52,** 2795–2807.

CASEY W. H., WESTRICH H. R., ARNOLD G. W., and BANFIELD J. F. (1989) The surface chemistry of dissolving labradorite feldspar. *Geochim. Cosmochim. Acta* **53,** 821–832.

CHOU L. and WOLLAST R. (1984) Study of the weathering of albite at room temperature and pressure with a fluidized bed reactor. *Geochim. Cosmochim. Acta* **48,** 2205–2218.

CHOU L. and WOLLAST R. (1985a) Steady-state kinetics and dissolution mechanisms of albite. *Amer. J. Sci.* **285,** 963–993.

CHOU L. and WOLLAST R. (1985b) Study of the weathering of albite at room temperature and pressure with a fluidized bed reactor. (Author's Reply) *Geochim. Cosmochim. Acta* **49,** 1659–1660.

CORRENS C. W. and VON ENGELHARDT W. (1938) Neue Untersuchungen über die Verwitterung des Kalifeldspates. *Chem. Erde* **12,** 1–22.

DIBBLE W. E., JR. and TILLER W. A. (1981) Non-equilibrium water/rock interactions—I. Model for interface-controlled reactions. *Geochim. Cosmochim. Acta* **45,** 79–92.

DOUGAN W. K. and WILSON A. L. (1974) The absorptiometric determination of aluminum in water. A comparison of some chromogenic reagents and the development of an improved technique. *Analyst* **99,** 413–430.

EGGLESTON C. M., HOCHELLA M. F., JR., and PARKS G. A. (1989) Sample preparation and aging effects on the initial dissolution rate and surface composition of diopside. *Geochim. Cosmochim. Acta* **53,** 797–804.

FREER R. (1981) Diffusion in silicate minerals and glasses: A data digest and guide to the literature. *Contrib. Mineral. Petrol.* **76,** 440–454.

FUNG P. C., BIRD G. W., MCINTYRE N. S., SANIPELLI G. G., and LOPATA V. J. (1980) Aspects of feldspar dissolution. *Nucl. Tech.* **51,** 188–196.

FURRER G. and STUMM W. (1986) The coordination chemistry of weathering: I. Dissolution kinetics of δ-Al_2O_3 and BeO. *Geochim. Cosmochim. Acta* **50,** 1847–1860.

GEISINGER K. L., GIBBS G. V., and NAVROTSKY A. (1985) A molecular orbital study of bond length and angle variations in framework structures. *Phys. Chem. Minerals* **11,** 266–283.

GIBBS G. V. (1982) Molecules as models for bonding in silicates. *Amer. Mineral.* **67,** 421–450.

GOOSSENS D. A., PHILIPPAERTS J. G., GIJBELS R., PIJPERS A. P., VAN TENDELOO S., and ALTHAUS E. (1989) A SIMS, XPS, SEM, TEM and FTIR study of feldspar surfaces after reacting with acid solutions. In *Water-Rock Interaction WRI-6* (ed. D. L. MILES), pp. 271–274. A. A. Balkema.

HELGESON H. C., MURPHY W. M., and AAGAARD P. (1984) Thermodynamic and kinetic constraints on reaction rates among minerals and aqueous solutions. II. Rate constants, effective surface area, and the hydrolysis of feldspar. *Geochim. Cosmochim. Acta* **48,** 2405–2432.

HELLMANN R., CRERAR D. A., and ZHANG R. (1989) Albite feldspar hydrolysis to 300°C. In *Reactivity of Solids* (eds. M. S. WHITTINGHAM, S. BERNASEK, A. J. JACOBSON, and A. NAVROTSKY); *Proceedings of the 11th International Symposium Princeton University, Part I,* pp. 314–329. Elsevier; also in *Solid State Ionics* (1989) **32/33,** 314–329.

HOCHELLA M. F., JR. (1988) Auger electron and X-ray photoelectron spectroscopies. In *Spectroscopic Methods in Mineralogy and Geology* (ed. F. C. HAWTHORNE); *Reviews in Mineralogy 18,* pp. 573–637. Mineral. Soc. Amer.

HOCHELLA M. F., JR. and BROWN G. E., JR. (1988) Aspects of silicate surface and bulk structure analysis using X-ray photoelectron spectroscopy (XPS). *Geochim. Cosmochim. Acta* **52,** 1641–1648.

HOCHELLA M. F., JR. and CARIM A. H. (1988) A reassessment of electron escape depths in silicon and thermally grown silicon dioxide thin films. *Surface Sci.* **197,** L260–L268.

HOCHELLA M. F., JR., PONADER H. B., TURNER A. M., and HARRIS D. W. (1988a) The complexity of mineral dissolution as viewed by high resolution scanning Auger microscopy: Labradorite under hydrothermal conditions. *Geochim. Cosmochim. Acta* **52,** 385–394.

HOCHELLA M. F., JR., LINDSAY J. R., MOSSOTTI V. G., and EGGLESTON C. M. (1988b) Sputter depth profiling in mineral surface analysis. *Amer. Mineral.* **73,** 1449–1456.

HOLDREN G. R., JR. and BERNER R. A. (1979) Mechanism of feldspar weathering—I. Experimental studies. *Geochim. Cosmochim. Acta* **43,** 1161–1171.

HOLDREN G. R., JR. and SPEYER P. M. (1985) pH dependent changes in the rates and stoichiometry of dissolution of an alkali feldspar at room temperature. *Amer. J. Sci.* **285,** 994–1026.

HUANG C. P. and STUMM W. (1973) Specific adsorption of cations on hydrous δ-Al_2O_3. *J. Colloid Interface Sci.* **43,** 409–420.

JAMBON A. and CARRON J. P. (1976) Diffusion of Na, K, Rb, and Cs in glasses of albite and orthoclase composition. *Geochim. Cosmochim. Acta* **40,** 897–903.

DE JONG B. H. W. S. and BROWN G. E., JR. (1980a) Polymerization of silicate and aluminate tetrahedra in glasses, melts, and aqueous solutions—I. Electronic structure of $H_6Si_2O_7$, $H_6AlSiO_7^-$, and $H_6Al_2O_7^{2-}$. *Geochim. Cosmochim. Acta* **44,** 491–511.

DE JONG B. H. W. S. and BROWN G. E., JR. (1980b) Polymerization of silicate and aluminate tetrahedra in glasses, melts, and aqueous solutions—II. The network modifying effects of Mg^{2+}, K^+, Na^+, H^+, OH^-, F^-, Cl^-, H_2O, CO_2 and H_3O^+. *Geochim. Cosmochim. Acta* **44,** 1627–1642.

KNAUSS K. G. and WOLERY T. J. (1986) Dependence of albite dissolution kinetics on pH and time at 25°C and 70°C. *Geochim. Cosmochim. Acta* **50,** 2481–2497.

LAGACHE M. (1965) Contribution à l'étude de l'altération des feldspaths, dans l'eau, entre 100 et 200°C, sous diverses pressions de CO_2, et application à la synthèse des minéraux argileux. *Bull. Soc. fr. Minéral. Cristallogr.* **LXXXVIII,** 223–253.

LAIDLER K. J. (1965) *Chemical Kinetics.* McGraw-Hill.

LASAGA A. C. (1981a) Rate laws of chemical reactions. In *Kinetics of Geochemical Processes* (eds. A. C. LASAGA and R. J. KIRKPATRICK); *Reviews in Mineralogy 8,* pp. 1–68. Mineral. Soc. Amer.

LASAGA A. C. (1981b) Transition state theory. In *Kinetics of Geochemical Processes* (eds. A. C. LASAGA and R. J. KIRKPATRICK); *Reviews in Mineralogy 8,* pp. 135–169. Mineral. Soc. Amer.

LIN T. H. and YUND R. A. (1972) Potassium and sodium self-diffusion in alkali feldspar. *Contrib. Mineral. Petrol.* **34,** 177–184.

LUCE R. W., BARTLETT R. W., and PARKS G. A. (1972) Dissolution kinetics of magnesium silicates. *Geochim. Cosmochim. Acta* **36,** 35–50.

MICHALSKE T. A. and FREIMAN (1983) A molecular mechanism for stress corrosion in vitreous silica. *J. Amer. Ceramic Soc.* **66,** 284–288.

MOGK D. W. and LOCKE W. W. (1988) Application of Auger Electron Spectroscopy (AES) to naturally weathered hornblende. *Geochim. Cosmochim. Acta* **52,** 2537–2542.

MURPHY W. M. and HELGESON H. C. (1987) Thermodynamic and kinetic constraints on reaction rates among minerals and aqueous solutions. III. Activated complexes and the pH-dependence of the rates of feldspar, pyroxene, wollastonite, and olivine hydrolysis. *Geochim. Cosmochim. Acta* **51,** 3137–3153.

NESBITT H. W. and MUIR I. J. (1988) SIMS depth profiles of weathered plagioclase, and processes affecting dissolved Al and Si in some acidic soil solutions. *Nature* **334,** 336–338.

PAČES T. (1973) Steady-state kinetics and equilibrium between ground water and granitic rock. *Geochim. Cosmochim. Acta* **37,** 2641–2663.

PARKS G. A. (1967) Aqueous surface chemistry of oxides and complex oxide minerals. In *Equilibrium Concepts in Natural Water Systems* (ed. W. STUMM); *Adv. Chem. Ser. 67,* pp. 121–160. Amer. Chem. Soc.

PECK J. A., FARNAN I., and STEBBINS J. F. (1988) Disordering and progress of hydration at the surface of diopside: A cross-polarization MAS NMR study. *Geochim. Cosmochim. Acta* **52,** 3017–3021.

PETIT J.-C., DELLA MEA G., DRAN J.-C., SCHOTT J., and BERNER R. A. (1987a) Mechanism of diopside dissolution from hydrogen depth profiling. *Nature* **325,** 705–707.

PETIT J.-C., DRAN J.-C., and DELLA MEA G. (1987b) Effects of ion plantation on the dissolution of minerals. Part II: Selective dissolution, *Bull. Mineral.* **110,** 25–42.

PETIT J.-C., DRAN J.-C., PACCAGNELLA A., and DELLA MEA G. (1989) Structural dependence of crystalline silicate hydration during aqueous dissolution. *Earth Planet. Sci. Lett.* **93,** 292–298.

PETIT J.-C., DRAN J.-C., SCHOTT J., and DELLA MEA G. (1989) New evidences on the dissolution mechanism of crystalline silicates by ion beam techniques. *Chem. Geology* **76,** 365–371.

PETROVIĆ R., BERNER R. A., and GOLDHABER M. B. (1976) Rate control in dissolution of alkali feldspars. I. Study of residual grains by X-ray photoelectron spectroscopy. *Geochim. Cosmochim. Acta* **40,** 537–548.

POSEY-DOWTY J., CRERAR D. A., HELLMANN R., and CHANG C. D. (1986) Kinetics of mineral-water reactions: theory, design and application of circulating hydrothermal equipment. *Amer. Mineral.* **71,** 85–94.

RIMSTIDT J. D. and BARNES H. L. (1980) The kinetics of silica-water reactions. *Geochim. Cosmochim. Acta* **44,** 1683–1699.

SCHINDLER P. W. (1981) Surface complexes at oxide-water interfaces. In *Adsorption of Inorganics at Solid Solution Interfaces* (eds. M. A. ANDERSON and A. J. RUBIN), pp. 1–49. Ann Arbor Science.

SCHINDLER P. W. and GAMSJÄGER H. (1972) Acid-base reactions of the TiO_2 (Anatase)-water interface and the point of zero charge of TiO_2 suspensions. *Kolloid-Z.Z. Polym.* **250,** 759–763.

SCHINDLER P. W. and STUMM W. (1987) The surface chemistry of oxides, hydroxides, and oxide minerals. In *Aquatic Surface Chemistry* (ed. W. STUMM), pp. 83–110. Wiley Interscience.

SCHOTT J. and BERNER R. A. (1983) X-ray photoelectron studies of the mechanism of iron silicate dissolution during weathering. *Geochim. Cosmochim. Acta* **47,** 2233–2240.

SCHOTT J. and PETIT J.-C. (1987) New evidence for the mechanisms of dissolution of silicate minerals. In *Aquatic Surface Chemistry* (ed. W. STUMM), pp. 293–315. Wiley Interscience.

SCHOTT J., BERNER R. A., and SJÖBERG E. L. (1981) Mechanism of pyroxene and amphibole weathering—I. Weathering studies of iron-free minerals. *Geochim. Cosmochim. Acta* **45,** 2123–2135.

SMETS B. M. J. and LOMMEN T. P. A. (1982) The leaching of sodium aluminosilicate glasses studied by secondary ion mass spectrometry. *Phys. Chem. Glasses* **23,** 83–87.

SMITH J. V. and BROWN W. L. (1988) *Feldspar Minerals 1. Crystal Structures, Physical, Chemical, and Microtextural Properties.* Springer-Verlag.

STRICKLAND J. D. H. and PARSONS T. R. (1972) Determination of reactive silicate. *Canada Fisheries Research Board Bull.* **167,** 65–70.

STUMM W. and FURRER G. (1987) The dissolution of oxides and aluminum silicates; examples of surface-coordination-controlled kinetics. In *Aquatic Surface Chemistry* (ed. W. STUMM), pp. 197–219. Wiley Interscience.

TAMM O. (1930) Experimentelle Studien über die Verwitterung und Tonbildung von Feldspaten. *Chem. Erde* **4,** 420–430.

TANUMA S., POWELL C. J., and PENN D. R. (1988) Proposed formula for electron inelastic mean free paths based on calculations for 31 materials. *Surface Sci. Lett.* **192,** L849–857.

WAGNER C. D., RIGGS W. M., DAVIS L. E., MOULDER J. F., and MUILENBERG G. E. (1978) *Handbook of X-Ray Photoelectron Spectroscopy.* Perkin-Elmer Corporation, Eden Prairie, Minnesota.

WEHRLI B. (1989) Surface structure and mineral dissolution kinetics: A Monte Carlo study. In *Water-Rock Interaction WRI-6* (ed. D. L. MILES), pp. 751–753. A. A. Balkema.

WILLIAMS E. L. and HECKMAN R. W. (1964) Sodium diffusion in soda-lime-aluminosilicate glasses. *Phys. Chem. Glasses* **5,** 166–171.

WOLLAST R. and CHOU L. (1985) Kinetic study of the dissolution of albite with a continuous flow-through fluidized bed reactor. In *The Chemistry of Weathering* (ed. J. I. DREVER); *NATO ASI Series, C 149,* pp. 75–96. D. Reidel.